

# Mathematical Metrology for Evaluating a 6DOF Visual Servoing System

Mili Shah  
Loyola Univ. Maryland  
Baltimore, Maryland  
mishah@loyola.edu

Tommy Chang, Tsai Hong  
National Inst. of Standards  
and Technology  
Gaithersburg, Maryland  
{tchang, hongt}@nist.gov

Roger Eastman  
Loyola Univ. Maryland  
Baltimore, Maryland  
reastman@loyola.edu

## ABSTRACT

In this paper we develop a homogeneous matrix transformation to fit two streams of dynamic six degree of freedom (6DOF) data for evaluating perception systems using ground truth. In particular, we compare object position and orientation results from a 6DOF laser tracker that we consider to be ground truth with results from a real-time visual servoing system from the Purdue Robot Vision Lab. A problem that arises when comparing these two data streams is that they are not necessarily in the same coordinate system. Therefore, a method to transform one coordinate system to the other is needed. We solve this problem by developing an optimization problem that minimizes the space between each coordinate system. In other words, we construct a rotation and translation which best transforms one coordinate space to the other.

## Categories and Subject Descriptors

C.4 [Performance of Systems]: Performance attributes; B.8.2 [Performance and Reliability]: Performance Analysis and Design Aids; G.1.6 [Optimization]: Global optimization; I.4.8 [Scene Analysis]: Motion, Tracking; I.5.4 [Applications]: Computer Vision

## General Terms

Computer Vision, Laser Tracker, Dynamic 6DOF metrology, Performance Evaluation

## 1. INTRODUCTION

In previous work [2] we reported on experiments in the evaluation of the performance of a real-time visual servoing system using a highly accurate, dynamic, six degree of freedom (6DOF) laser tracker. The purpose of the experiments was to demonstrate a method for evaluating real-time 6DOF dimensional measurements of an object or assembly component under moderately constrained motion. By taking geometrically calibrated, time-synchronized data streams si-

multaneously from the 6DOF servoing sensor system and the laser tracker, the 6DOF system data can be evaluated against the laser data serving as conventional ground truth. In this paper we report on improved techniques for post-experiment and geometric calibration and evaluation of the experimental data.

Reliable, accurate real-time systems for 6DOF perception would have applications in advanced manufacturing robotics and automation, as they would enable greater interaction with objects in motion and more flexible robotic workcells. However, despite considerable advances in real-time vision and in laboratory demonstrations [7,16,17], these systems have not yet been widely commercialized and this would be assisted by reference metrology systems for empirical performance evaluation. Reference systems would include a standard sensor system for ground truth along with appropriate metrics for the comparison of test systems with the reference system. Standards and test procedures for dimensional metrology are well-established and highly accurate for static measurements, with coordinate measuring machines and laser trackers giving position measurements to microns. However, the theory, technology, and test procedures are not well established for dynamic dimensional measurements in uncontrolled environments.

To assist in establishing these test procedures, the questions addressed in this work focus on calibrating and comparing two 6DOF data streams. We assume the two vector data streams include position as X, Y, Z, pose as roll, pitch and yaw, and that the two data streams have been time-synchronized so we have correspondence between individual vectors in each data stream. But, we do not assume accurate geometric calibration of coordinate systems between the two data streams. During our initial experiments, accurate calibration proved difficult so we looked for a post-experiment calibration approach that would compute an accurate transformation between two coordinate systems, taking into account all information in the 6DOF data. Once the two data streams have been calibrated, we wish to compare the two for the magnitude and nature of the differences in order to characterize the 6DOF system under test.

The real-time visual servoing implementation used in this study was developed at the Purdue Robot Vision Lab<sup>1</sup> us-

(c) 2009 Association for Computing Machinery. ACM acknowledges that this contribution was authored or co-authored by a contractor or affiliate of the U.S. Government. As such, the Government retains a nonexclusive, royalty-free right to publish or reproduce this article, or to allow others to do so, for Government purposes only.

PerMIS '09, September 21-23, 2009, Gaithersburg, MD, USA  
Copyright 2009 ACM 978-1-60558-747-9/09/09 ...\$10.00.

<sup>1</sup>Certain commercial equipment, instruments, or materials are identified in this paper in order to adequately specify the experimental procedure. Such identification does not imply recommendation or endorsement by NIST nor does it imply that the materials or equipment identified are necessarily the best for the purpose.

ing a subsumptive, hierarchical, and distributed vision-based architecture for smart robotics [3,6,16,17]. This is a robust, advanced dynamic visual servoing implementation with a high-level of fault tolerance to non-cooperative conditions such as severe occlusions and sudden illumination changes. The Purdue system combines a ceiling mounted camera with a trinocular system mounted on the robot end-effector, and uses position based visual servoing (PBVS). The work in this paper is aimed at the evaluation of sensors for PBVS, in which the servoing system senses the position and orientation of the part in 3D coordinates, as opposed to image based visual servoing (IBVS), in which the servoing system senses the position and orientation of the part in 2D image coordinates.

## 2. PREVIOUS WORK

While pose estimation and visual servoing receive attention in the literature, evaluation of visual servoing usually appears as a secondary element to the presentation of new servoing approaches or algorithms. Many papers that present a new approach include an empirical evaluation, but since the paper emphasizes the development of the new approach, the evaluation section is often brief. Two papers that do focus on the evaluation of visual servoing algorithms are [1, 5]. In [5], there is a sensitivity analysis and simulation to compute the contribution of image measurement errors to the calculated pose and control trajectory for PBVS and hybrid visual servoing. In [1], there is a modular analysis of the elements of a visual servoing systems with the intention of supporting a design and evaluation framework, with an emphasis on the control subsystem. The paper considers many aspects of performance analysis for static and dynamic cases, as well as accuracy and timing issues.

Most evaluation papers consider static pose only [6, 8] and not 6DOF sensor measurements under motion. References [8, 9] use Monte Carlo simulation for the evaluation of pose algorithm accuracy under noise and object orientations. In those articles, results are given for pose estimation for a complex industrial part and the error from unidentified ground truth is plotted as position or orientation error vs. the rotation of the object. The key result is to note that the error as a function of part rotation varies considerably, spiking at ambiguous orientations of the object. Two papers that do consider dynamic pose are [7, 11]. In [11] disassembly used car parts video sequences are used for tests of a model-based algorithm with four parameter variations to analyze the relative contributions of subcomponents such as the edge detection operator or search technique. The results are given as deviations from the results of the one parameter set that successfully maintained track through the video sequences, but the nature and quality of this retrospective ground truth is not described in the article. In [11] three tracking approaches for 6DOF pose estimation and grasping of hand-held objects are evaluated using ground truth from an unidentified infrared marker tracking system good to 1.5 m in position but with no rotation accuracy or measurements per second cited. The three approaches run at between 8 Hz and 25 Hz. The article gives results in graphs that compare ground truth position and orientation data to robot end-effector position and tracked position, but no quantitative or summary statistics are given for the graphed data.

The metrics used to evaluate pose estimation and visual

servoing systems vary. They include the mean and standard deviation of a measure of error in world coordinates, including individual differences for each coordinate, a norm for position and orientation separately, and rarely a combined norm for all 6 degrees of freedom. The orientation can be compared in roll-pitch-yaw, quaternion, or angle-axis representations. In experiments without ground truth in world coordinates, or for IBVS in which pose in world coordinates is not computed, errors are computed in the image domain. In some visual servoing evaluations, the metric is the number of cases successfully completed during the experiments. In physical experiments in the evaluation of pose estimation or visual servoing, a mechanism must be used to generate motion, frequently a robot arm [3, 4, 11]. [11] uses an arm to move a camera towards a car battery through a known trajectory linear in both translation and angle, and repeats the motion 80 times to judge repeatability of the tracking algorithm.

## 3. VISUAL SERVOING EXPERIMENTS

### 3.1 Purdue Data

The Purdue system produces a 6DOF pose at the rate of 30 Hz. The output consists of 3 translations and 3 rotational angles, all relative to the robot base frame. The object whose pose is measured by the Purdue system, is a typical engine cover about 0.5 m in width and 0.25 m in height. Figure 1 defines the object frame.

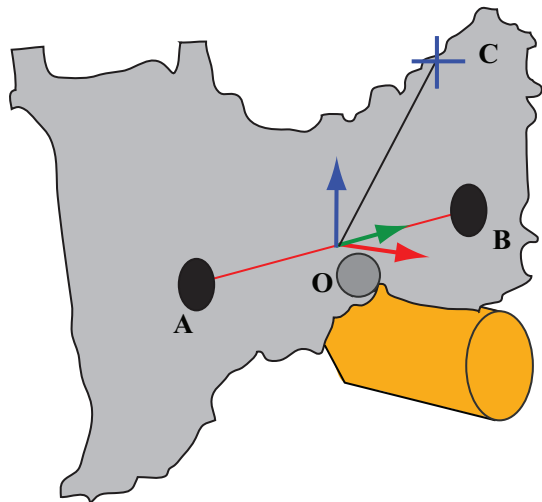


**Figure 1: Engine cover and the object frame: A,B and C are coplanar in the YZ plane. O is centered between A and B. OB is the Y axis, while the X-axis is in the direction of the cross product of OB and OC. The Z-axis is given by the cross product of axes X and Y.**

### 3.2 Laser Tracker Data

The laser tracker (LT) measures the 3D locations of a smart track sensor (STS), which measures its own orientation. Together, the two measurements give a complete 6DOF pose of the STS at a rate of up to 150 Hz.

In our experiments, the STS is rigidly attached beneath the engine cover (object) as shown in Figure 2. The laser



Figure 2: Engine cover (object) and the STS

tracker measures the position and orientation of the STS, while the Purdue system measures the position and orientation of the engine cover (object). However, since the STS and the engine cover (object) are fixed rigidly to each other, the laser tracker can be utilized to compute the transformation between the two. A point of concern is that the Purdue data is in the coordinate system of the robot base whereas the laser tracker has its own coordinate system. Calibrating these two coordinate systems can be a daunting task. Therefore, the objective of this paper is to use the data to construct the best transformation of the robot base coordinate system into the laser tracker coordinate system. The methodology of this process is shown in Section 5.

### 3.3 Synchronization of the two systems

In order to achieve a matched-pairs design, we take simultaneous measurements and thus minimize the difference in system outputs due to independent measurements taken at different times and different rates. Another advantage of taking simultaneous measurements is that we do not need to know the object motion.

Synchronization can be easily achieved through a common external signal to trigger data acquisition. We use a 30 Hz square wave signal as the Purdue system requires a steady 30 Hz data stream (limited by the cameras' frame rate).

Although a common external trigger signal is used to trigger the data acquisition of both systems, the Purdue system does not latch data instantly. This is because the cameras in the Purdue system do not use a fixed shutter/exposure time. After a trigger signal is received, the cameras open their shutters for some amount of time to collect light. In general, the amount of time changes from frame to frame, depending on the lighting condition at the time. During this exposure/integration time, motion blur can happen. Al-

though the integration time is small, it can be a source of uncertainty in determining the exact pose of the object. Large motion blur will increase pose uncertainty.

In order to be able to uniquely identify and track each trigger signal, the data collection software from each system maintains its own sequence counter and tags each count with a time-stamp having microsecond resolution. Both data collection software modules get their timestamps indirectly from a common clock source via an Network Time Protocol (NTP) server. However, instead of running an NTP client, which attempts to model the clock drift over a long period of time, we simply have the data collection computers synchronize the NTP sever every 10 s. We find this setup allows our data collection computers to stay synchronized to each other within 3 ms. In general, the clock circuits in today's consumer computers are precise but temperature dependent.

## 3.4 Experimental Setups

We conducted two sets of experiments, one with the object stationary and one with the object moving with a simple linear velocity.

### 3.4.1 Stationary Tests

The stationary tests allowed us to evaluate the basic performance of both systems and assure that the laser tracker was performing to specification after shipping. The object was placed in four positions and data were collected for 15 s to 30 s each.

### 3.4.2 Linear Motion Tests

In the linear motion tests, the object was moved about 1.5 m left to right. For each trial, the motion was repeated 30 times as the object moved.

## 4. CALIBRATION

In order to compare data streams collected from the Purdue system with data streams collected from the laser tracker system, which we consider to be ground truth, both systems must first be placed in the same coordinate system. In other words, a homogeneous matrix that transforms the Purdue data into the coordinate system of the laser tracker system data is needed. We define  ${}_X\mathbf{H}_Y$  as the homogeneous transformation from the coordinate system of Y to X. In other words,  ${}_X\mathbf{H}_Y$  defines the 6DOF pose of Y in X coordinates. Therefore in this paper, we are searching for  ${}_{LT}\mathbf{H}_{RB}$  where LT is the output of the laser tracker system and RB is the output of the Purdue system. In [2], a description of the methodology for the output of both the Purdue system and the laser tracker system is provided. A review is given in Section 3. Here, we will give an overview of the necessary components (Figure 3).

The Purdue system provides  ${}_{RB}\mathbf{H}_O$ , where RB denotes the robot base and O denotes the object of interest. Similarly, the laser tracker system provides  ${}_{LT}\mathbf{H}_{STS}$ . However,  ${}_{LT}\mathbf{H}_O$  is what is needed. This can be calculated by noting that

$${}_{LT}\mathbf{H}_O = {}_{LT}\mathbf{H}_{STS} \times {}_{STS}\mathbf{H}_O \quad (1)$$

and

$${}_{STS}\mathbf{H}_O = {}_{STS}\mathbf{H}_{LT} \times {}_{LT}\mathbf{H}_O \quad (2)$$

is a fixed value and thus only one coordinate frame is needed to construct it.  ${}_{STS}\mathbf{H}_{LT} = ({}_{LT}\mathbf{H}_{STS})^{-1}$  and  ${}_{LT}\mathbf{H}_O$  is constructed by using the laser tracker along with a spherically

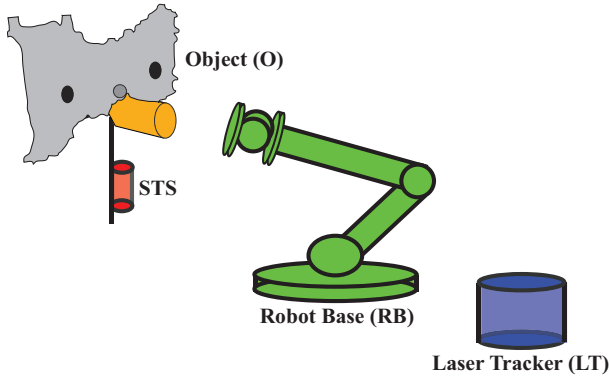


**Figure 3: The necessary components of the Purdue data stream and the laser tracker data stream.**

mounted reflector (SMR) to calculate the Cartesian coordinate position of three features on the object. These three features are enough information to identify the object's reference frame [2].

The output for the laser tracker system is  ${}_{LT}\mathbf{H}_O$  whereas the output for the Purdue system is  ${}_{RB}\mathbf{H}_O$ . Therefore, to be able to compare the two outputs  ${}_{LT}\mathbf{H}_{RB}$  is needed. The following section describes a mathematical method that constructs  ${}_{LT}\mathbf{H}_{RB}$  by forming the best homogeneous matrix that fits the data  ${}_{RB}\mathbf{H}_O$  from the Purdue system to the  ${}_{LT}\mathbf{H}_O$  of the laser tracker system.

## 5. MATHEMATICAL ANALYSIS

### 5.1 Homogeneous Matrix

In the previous section, an overview of how the data streams are constructed from both the Purdue system and the laser tracker system is given. The output of the Purdue system is given as a series of homogeneous matrices

$$({}_{RB}\mathbf{H}_O)_i = \begin{bmatrix} \widehat{\mathbf{R}}_i & \widehat{t}_i \\ 0 & 1 \end{bmatrix} \quad (3)$$

for time steps  $i = 0, 1, \dots, n-1$ . Similarly, the output of the laser tracker system is a series of homogeneous matrices

$$({}_{LT}\mathbf{H}_O)_i = \begin{bmatrix} \mathbf{R}_i & t_i \\ 0 & 1 \end{bmatrix} \quad (4)$$

for time steps  $i = 0, 1, \dots, n-1$ . We are interested in finding a rotation  $\mathbf{R}$  and translation  $\mathbf{t}$  that best transforms the coordinate system of the Purdue data into the coordinate system of the laser tracker data. Specifically, we want to construct the homogeneous matrix

$$\mathbf{H} = \begin{bmatrix} \mathbf{R} & \mathbf{t} \\ 0 & 1 \end{bmatrix}$$

that solves

$$\min_{\mathbf{H}} \|\mathbf{H}\mathbf{P} - \mathbf{L}\|^2$$

where

$$\mathbf{P} = [({}_{RB}\mathbf{H}_O)_0 \quad ({}_{RB}\mathbf{H}_O)_1 \quad \dots \quad ({}_{RB}\mathbf{H}_O)_{n-1}]$$

and

$$\mathbf{L} = [({}_{LT}\mathbf{H}_O)_0 \quad ({}_{LT}\mathbf{H}_O)_1 \quad \dots \quad ({}_{LT}\mathbf{H}_O)_{n-1}].$$

Shah develops an algorithm for constructing such an  $\mathbf{H}$  in [10]. Specifically, the best rotation has to first be constructed as

$$\mathbf{R} = \mathbf{V}\mathbf{D}\mathbf{U}^T$$

where the singular value decomposition of

$$\mathbf{X}\widehat{\mathbf{X}}^T = \mathbf{U}\mathbf{S}\mathbf{V}^T$$

with

$$\mathbf{X} = [\mathbf{R}_0 \quad t_0 \quad \dots \quad \mathbf{R}_{n-1} \quad t_{n-1}]$$

$$\widehat{\mathbf{X}} = [\widehat{\mathbf{R}}_0 \quad \widehat{t}_0 \quad \dots \quad \widehat{\mathbf{R}}_{n-1} \quad \widehat{t}_{n-1}]$$

and

$$t_i = t_i - t \quad \text{with} \quad t = \frac{1}{n} \sum_{i=0}^{n-1} t_i \quad (5)$$

$$\widehat{t}_i = \widehat{t}_i - \widehat{t} \quad \text{with} \quad \widehat{t} = \frac{1}{n} \sum_{i=0}^{n-1} \widehat{t}_i. \quad (6)$$

Also

$$\mathbf{D} = \begin{cases} \text{diag}(1, 1, 1) & \text{if } \det(\mathbf{V}\mathbf{U}^T) = 1, \\ \text{diag}(1, 1, -1) & \text{if } \det(\mathbf{V}\mathbf{U}^T) = -1. \end{cases}$$

Once the rotation  $\mathbf{R}$  is found, the translation  $\mathbf{t}$  can be constructed by setting

$$\mathbf{t} = \widehat{\mathbf{t}} - \mathbf{R}\widehat{\mathbf{t}}$$

where  $t$  and  $\widehat{t}$  are defined in (5) and (6), respectively.

### 5.2 Error Metrics

Given a general homogeneous matrix  $\mathbf{H}$  – made up of a rotation  $\mathbf{R}$  and translation  $\mathbf{t}$  – a series of metrics is now offered to compare how well  $\mathbf{H}$  transforms a given data stream into another [10].

To see how well a given rotation  $\mathbf{R}$  transforms a single rotation  $\mathbf{R}_i$  from the laser tracker data stream to a rotation  $\widehat{\mathbf{R}}_i$  from the Purdue data stream, evaluate

$$\begin{aligned} \|\mathbf{R}\mathbf{R}_i - \widehat{\mathbf{R}}_i\|^2 &= \|\mathbf{R}\mathbf{R}_i\|^2 - 2\text{tr}(\mathbf{R}\mathbf{R}_i\widehat{\mathbf{R}}_i^T) + \|\widehat{\mathbf{R}}_i\|^2 \\ &= 6 - 2(1 + 2\cos\theta) \end{aligned}$$

where  $\{1, \cos\theta \pm i\sin\theta\}$  are the eigenvalues of  $\mathbf{R}\mathbf{R}_i\widehat{\mathbf{R}}_i^T$ . Therefore,

$$0 \leq \|\mathbf{R}\mathbf{R}_i - \widehat{\mathbf{R}}_i\|^2 \leq 8,$$

since  $-1 \leq \cos\theta \leq 1$ . Moreover,

$$0 \leq 1 - \frac{1}{8}\|\mathbf{R}\mathbf{R}_i - \widehat{\mathbf{R}}_i\|^2 \leq 1.$$

defines a metric between 0 and 1 where 1 denotes a perfect fit.

A similar metric can be constructed to compare a given translation  $t_i$  from the laser tracker data stream to a translation  $\widehat{t}_i$  from the Purdue data stream. In this case we want to see how close  $\mathbf{R}t_i + \mathbf{t}$  is to  $\widehat{t}_i$ . Thus, we consider the dot product between these two normalized vectors. In other words, we evaluate

$$0 \leq \frac{(\mathbf{R}t_i + \mathbf{t})^T \widehat{t}_i}{\|\mathbf{R}t_i + \mathbf{t}\| \|\widehat{t}_i\|} \leq 1$$

Once again this defines a metric with values between 0 and 1 where 1 denotes a perfect fit. One should note that this metric loses valuable information regarding the scaling of the problem. For example, if the vectors  $\mathbf{R}t_i + \mathbf{t}$  and  $\hat{t}_i$  point in the same direction (not necessarily the same magnitude), then the metric would give an accuracy reading of 1, though the vectors may not be equal. However, this metric is problem independent allowing one to compare two different problem setups. Another metric that can be used (but is problem dependent) is to look at

$$\|\mathbf{R}t_i + \mathbf{t} - \hat{t}_i\|.$$

However, this metric does not have a defined upper bound. Instead, one could compare the magnitude of this metric with the magnitude of the data used in order to calculate the accuracy of the algorithm.

In the next section, experiments will be performed to see how well the homogeneous matrix constructed in 5.1 performs using the metrics just defined.

## 6. EXPERIMENTS

The algorithm in 5.1 that constructed the best homogeneous matrix  $\mathbf{H}$  to fit two streams of 6DOF data was applied to data streams that were collected from the Purdue system and a laser tracker system at Purdue University in April of 2008 [2]. These data streams were obtained from two experiments (see Section 3).

### 6.1 Stationary

In the stationary experiment, the object was placed in four positions for 15 s to 30 s each. The mean distance for each position was in the 3500 mm to 4100 mm range with a standard deviation of 0.006 to 0.008 for the STS/LT system. For the Purdue Line tracker system each position was in the 2600 mm to 2700 mm range with a standard deviation of 0.560 to 0.630 standard deviation. More details can be found in [2]. Overall, the laser tracker system is two orders of magnitude more accurate than the Purdue system.

The homogeneous matrix calculated from these stationary data streams is

$$\mathbf{H}_{\text{Stat}} = \begin{bmatrix} -0.79 & -0.61 & -0.11 & 715.94 \\ 0.60 & -0.79 & 0.07 & 2228.30 \\ -0.13 & -0.01 & 0.99 & -1133.76 \\ 0 & 0 & 0 & 1 \end{bmatrix}.$$

We calculated the accuracy of this homogeneous matrix using the metrics provided in the previous section. Not surprisingly, we have near 100 % accuracy for this homogeneous matrix for both the rotation and translation as can be seen in Figure 4. In addition, the translational error is around 12 mm – a two order decrease in magnitude compared to the data position.

### 6.2 Linear Motion

In the linear motion experiment, the object was moved 1.5 m to the left and right. This motion was repeated 30 times for each trial and quickly returned back to the starting position. It should be noted that this backward sweep was ignored in the data collection for both systems.

The homogeneous matrix calculated from these linear mo-

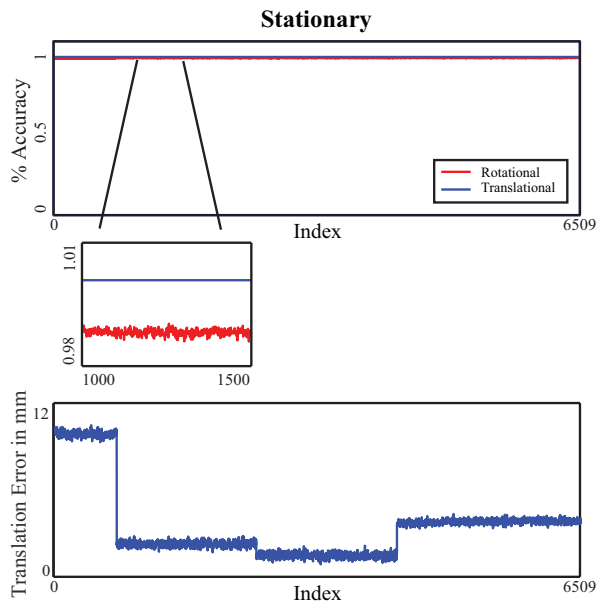


**Figure 4: Error metrics from the stationary experiment where the object was placed in four positions for 15 s to 30 s each.**

tion data streams is

$$\mathbf{H}_{\text{Move}} = \begin{bmatrix} -0.79 & -0.61 & -0.08 & 666.20 \\ 0.61 & -0.79 & 0.04 & 2271.00 \\ -0.09 & -0.01 & 1.00 & -1238.45 \\ 0 & 0 & 0 & 1 \end{bmatrix}$$

which is not very different from the stationary homogeneous matrix  $\mathbf{H}_{\text{Stat}}$ . This should be expected since this experiment should not have much noise introduced from the simple linear motion. Moreover, the minimal noise results in  $\mathbf{H}_{\text{Move}}$  having near 100 % accuracy for both the rotation and translation as can be seen in Figure 5. In addition, the translational error is only around 10 mm.

## 7. CONCLUSIONS

In this paper, we presented improved techniques for the calibration of two 6DOF data streams. Previously, calibration was done by hand which was prone to errors. Here, the data was used to mathematically find the best fit between two given 6DOF data streams. Specifically, we constructed the homogeneous matrix that best transformed the coordinate system of one of the two data streams into the other. Moreover, metrics were offered to evaluate the effectiveness of this transformation.

We tested this method on two data sets collected at Purdue University. The first consisted of the object being placed in four positions for 15 s to 30 s and the second consisted of the object moving in a linear motion. We found that the homogeneous matrix fit the data almost perfectly for these two systems.

## 8. ACKNOWLEDGMENTS

We thank Mike Shneier and Elena Messina for their fruitful discussions. We thank Avi Kak, Johnny Park, and Ger-

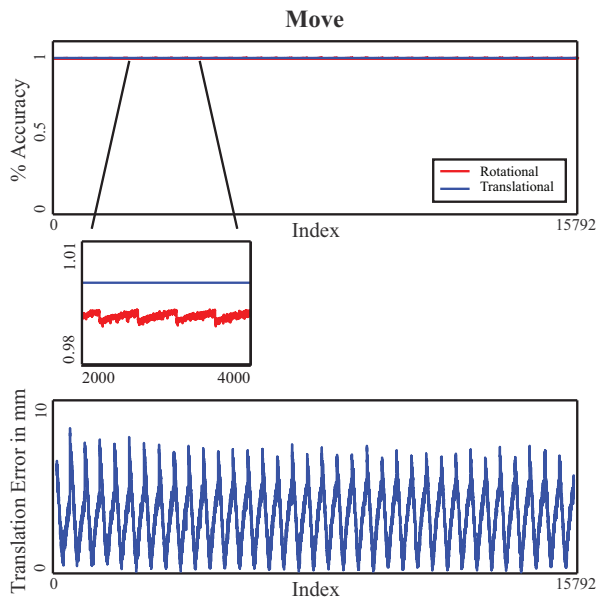


**Figure 5: Error metrics from the move experiment where the object was moved 1.5 m to the left and right.**

man Holguin from Purdue University for working with us on the real-time data collection using their vision system, robot arm, and rail. In addition, we would like to thank Jane Shi from General Motors, Frank Maslar from Ford, and Kam Lau from Automated Precision Inc. for their collaboration.

## 9. REFERENCES

- [1] M. Bachiller, J. A. Cerrada, and C. Cerrada. A modular scheme for controller design and performance evaluation in 3d visual servoing. *Journal of Intelligent and Robotics Systems*, 36(3):235–264, 2003.
- [2] T. Chang, T. Hong, M. Shneier, G. Holguin, J. Park, and R. Eastman. Dynamic 6dof metrology for evaluating a visual servoing system. In *Performance Metrics for Intelligent Systems (PerMIS) Workshop*, pages 173–180, 2008.
- [3] K. Deguchi. A direct interpretation of dynamic images with camera and object motions for vision guided robot control. *International Journal of Computer Vision*, 37(1):7–20, 2000.
- [4] B. Espiau. Effect of camera calibration errors on visual servoing in robotics. In *International Symposium on Experimental Robotics*, pages 182–192, 1993.
- [5] V. Kyrki, D. Kragic, and H. I. Christensen. Measurement errors in visual servoing. *Robotics and Autonomous Systems*, 54(10):815–827, 2006.
- [6] C. B. Madsen. Viewpoint variation in the noise sensitivity of pose estimation. In *Conference on Computer Vision and Pattern Recognition*, pages 41–46, 1996.
- [7] P. Preisig and D. Kragic. Robust statistics for 3d object tracking. In *International Conference on Robotics and Automation*, pages 2403–2408. IEEE, 2006.

- [8] G. J. Reid, J. Tang, and L. Zhi. A complete symbolic-numeric linear method for camera pose determination. In *ISSAC*, pages 215–223, 2003.
- [9] A. H. Rivera-Ríos, F.-L. Shih, and M. M. Marefat. Stereo camera pose determination with error reduction and tolerance satisfaction for dimensional measurements. In *International Conference on Robotics and Automation*, pages 423–428, 2005.
- [10] M. I. Shah. Six degree of freedom point correspondences. Technical report, Department of Mathematical Sciences, Loyola College in Maryland, 2009.
- [11] M. Tonko and H.-H. Nagel. Model-based stereo-tracking of non-polyhedral objects for automatic disassembly experiments. *International Journal of Computer Vision*, 37(1):99–118, 2000.